Journal of Materials Chemistry C

ROYAL SOCIETY OF CHEMISTRY

PAPER

View Article Online
View Journal | View Issue

Cite this: J. Mater. Chem. C, 2023, 11, 4937

One- and two-photon lasing from a TCF-based AIE dye†

Kamila Lupinska, *[a] Martyna Durko-Maciag, [a] Chantal Andraud, [b] Yann Bretonnière, [b] Piotr Hanczyc, [c] Piotr Fita, [c] Piotr Szulim, [c] Jaroslaw Mysliwiec [a] and Lech Sznitko *[a]

The 2,4,6-OMe-TCF dye, exhibiting the aggregation-induced emission (AIE) phenomenon, is investigated according to the generation of laser light. Light amplification is possible only for concentrated solutions with dye amounts close to the saturation level, indicating that the aggregation process plays an essential role in establishing light enhancement. Moreover, lasing is also achievable for the powdered form of the dye, with the clearly evident presence of nano- and micro-crystals; however, in this case, the spectral position of a gain profile is considerably red-shifted. The aggregation caused by a non-solvent addition to a dye solution can increase the average random lasing (RL) emission intensity even by a factor of 170 for the band assigned to aggregates. The dye can serve as a very versatile lasing material; it could be used in the form of a liquid solution as well as a dopant for polymeric matrices. It can be easily processed from solutions; therefore, it perfectly matches the requirements of novel types of soft and elastic materials for printed optoelectronics. Finally, the molecular disorder present in polymeric systems involving the existence of the dye in molecular, aggregated, and crystalline forms can result in the generation of two-photon excited laser emission. We believe that the synthesis of molecular systems exhibiting increased emission quantum yields both in aggregated and crystalline forms may become a common strategy to obtain efficient, multiphoton-excited organic laser materials.

Received 3rd November 2022,
Accepted 15th March 2023

DOI: 10.1039/d2tc04673c

rsc.li/materials-c

Introduction

Since the discovery of dyes exhibiting the aggregation-induced emission (AIE) phenomenon, many scientific groups have extensively studied these types of molecules. They can exhibit many advantageous properties due to which they have found many potential applications, for example, in optoelectronics as materials for organic light-emitting diodes (OLEDs),[1–3] solar concentrators,[4,5] light-emitting liquid crystal displays (LE-LCDs),[6] or even as components for electrochromic devices.[7–9] Next to optoelectronics, AIE dyes also proved their utility in sensing,[1,9–11] bio-imaging,[12–14] and anti-counterfeiting applications.[15]

However, despite the great interest in these compounds, the AIE effect on lasing properties is not well described yet. Some papers report on light amplification[16–25] but without general discussion on how this phenomenon can influence light enhancement. Therefore, in this article, we want to investigate how the AIE effect can affect the lasing properties of luminescent materials. We hypothesize that this process might be crucial in establishing light amplification, and if the luminescent molecule is showing remarkable emission in the crystalline form, the crystallization of a dye might also be used to tailor the lasing properties of the resulting material. Moreover, what could be even more significant is that the AIE dopants may play a key role in developing a strategy for designing multiphoton–excited laser materials. The last hypothesis is drawn based on the fact that AIE dyes have already proven their outstanding nonlinear optical (NLO) properties, including NLO absorption and excitation.[13,14]

We focused our attention on the 2,4,6-OMe-TCF dye to test the above-mentioned hypotheses. The molecule is shown in Fig. 1 (a), and it was previously described in ref. 26. It represents a group of small molecular systems with a typical push–pull design, where one part of the molecule serves as a donor of electrons, and the second one plays the role of an electron acceptor. Such kinds of compounds are still attracting much attention from the scientific community. The simple, efficient, and cost-effective synthesis is one of the most important advantages of these systems.

[a] Institute of Advanced Materials, Faculty of Chemistry, Wroclaw University of Science and Technology, Wybrzeze Wyspianskiego 27, 50-370 Wroclaw, Poland. E-mail: lech.sznitko@pwr.edu.pl, kamila.lupinska@pwr.edu.pl
[b] Univ Lyon, ENS de Lyon, CNRS UMR 5182, Laboratoire de Chimie, F69342, Lyon, France
[c] Institute of Experimental Physics, Faculty of Physics, University of Warsaw, 02-093 Warsaw, Pasteura 5, 02-093 Warsaw, Poland

† Electronic supplementary information (ESI) available. See DOI: https://doi.org/10.1039/d2tc04673c

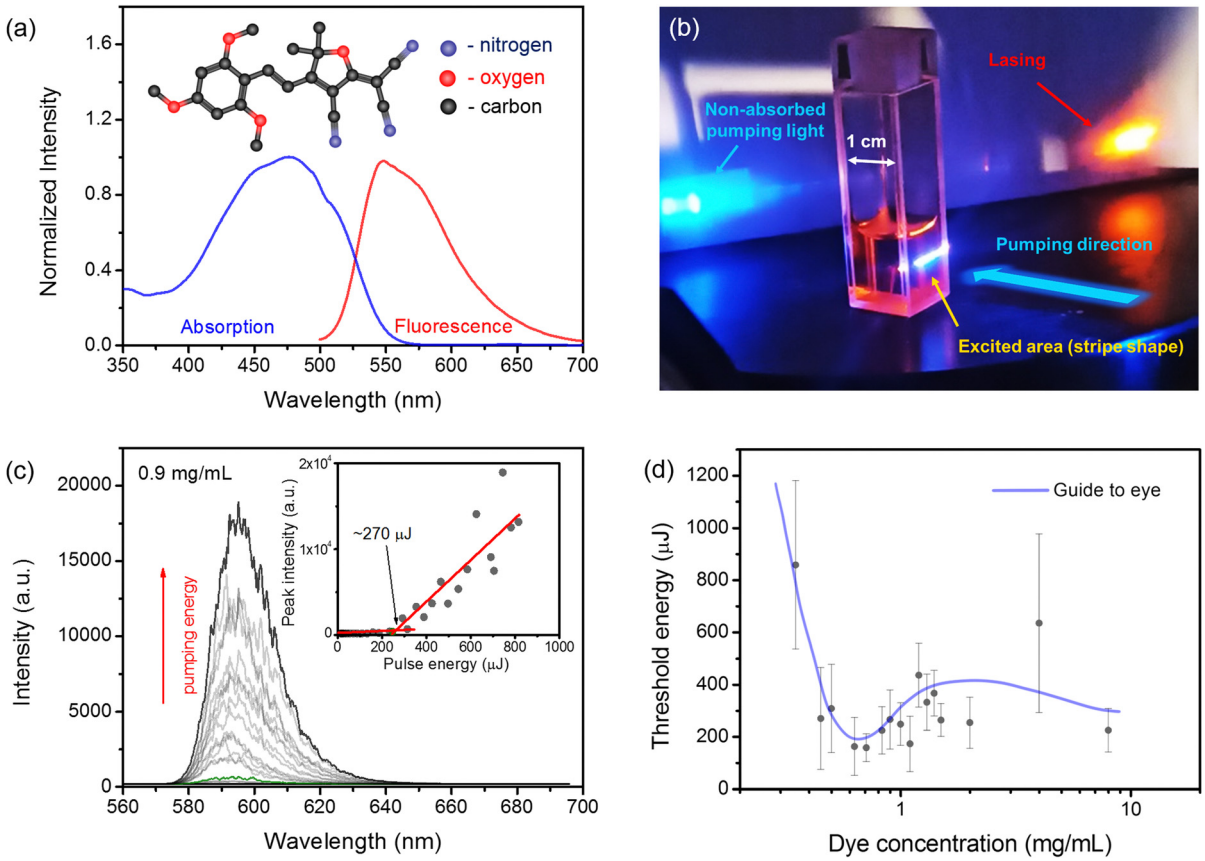

Fig. 1 Absorption and emission spectra of 2,4,6-OMe-TCF dye in THF solution with its molecular structure (a). A photograph of the laser emission from 2,4,6-OMe-TCF in THF solution (b). Typical evolution of the RL spectrum upon increasing pumping energy, the inset shows peaks intensity of RL *vs.* pumping pulse energy with the lasing threshold at around 270 μJ, which corresponds to 54 kW of pumping power (c). The energy threshold of the lasing as a function of the dye concentration in THF, the blue curve, is a guide to the eye (d).

Nowadays, a vast number of dyes are designed in such a way that they can exhibit many desired and attractive features like AIE,[27,28] photoisomerization,[29,30] ability to generate NLO effects,[31] *etc.* Among them, one can distinguish the dyes containing the 2-dicyanomethylidene-3-cyano-4,5,5-trimethyl-2,5-dihydrofuran or tricyanofuran (TCF) group, which is one of the strongest electron-withdrawing moieties.[32] The title molecule represents a wide family of TCF derivatives. Utilization of this moiety in a molecule with the push–pull design can significantly enlarge the Stokes shift of emission and introduce a remarkable NLO response. As was recently shown by Ipuy *et al.*, such compounds can show excellent linear and nonlinear optical properties, and what is more interesting is that they can exhibit the AIE phenomenon as well.[26]

The 2,4,6-OMe-TCF dye was selected for measurements because it shows a remarkable AIE behavior. It leads to a significant increase in emission efficiency and a drastic change in the emission spectrum[13,26] as a result of aggregation and further crystallization. This AIE-like behavior can be ascribed to the formation of dye aggregates as well as recrystallization. Both aggregated and crystalline forms exhibit relatively high emission quantum yields equal to 7 and 22%, respectively.[26] Moreover, this compound can be used to fabricate so-called fluorescent organic nanoparticles (FONs), both in amorphous and crystalline forms. Such FONs can be used as efficient two-photon excited emitters, which are especially desirable for two-photon imaging of biological tissues.[13]

This article shows that the 2,4,6-OMe-TCF molecule is a versatile laser compound. It can be used to design laser materials of outstanding performance, both in the form of liquid solutions and polymeric solid layers. The aggregates formed during the dye precipitation can even boost the lasing intensity up to ~170 times. Moreover, the formation of mesoscopic-size crystals can be responsible for two-photon excited lasing (2PEL) in polymeric layers.

Results

At first, the absorption and emission spectra of the tetrahydrofuran (THF) dissolved TCF dye (2.6×10^{-5} M) were investigated. We monitored the absorption spectrum to select the appropriate excitation wavelength for one-photon excited lasing (1PEL). The photoluminescence (PL) spectrum was recorded to establish the spectral range of potential laser emission occurrence. Experimental details are available in the Materials and methods section in the ESI.† We found that the main

absorption band spans from nearly 400 nm to 550 nm, with a maximum placed at around 477 nm. The fluorescence spectrum was measured from 500 nm to around 700 nm. In this range, it has a maximum located at 548 nm, the full width at half of the maximum (FWHM) of emission is equal to 75 nm and the Stokes shift is 71 nm. The normalized absorption and emission spectra are shown in Fig. 1 (a).

Next, we utilized the nanosecond pulse laser beam to excite the THF solutions containing different amounts of the TCF dye. The experimental setup is described in the Materials and Methods section in the ESI.† An example of 1PEL from a cuvette filled with a TCF solution is shown in Fig. 1(b). Our measurements were carried out in a wide range of TCF dye concentrations in the THF solvent (from 0.1 mg mL^{-1} to 8 mg mL^{-1}). Such highly concentrated solutions were selected because we wanted to check the influence of the aggregation/crystallization effect on laser emission. The stimulated emission was obtained only for samples with dye concentrations higher or equal to 0.35 mg mL^{-1}. Typically, the laser emission was evident above a certain energy threshold level and was visualized as a band (located at ~595 nm with FWHM ~20 nm) composed of multiple narrow modes randomly appearing in the spectrum. According to the literature, for such highly concentrated solutions, even the presence of small aggregates can be responsible for random feedback formation.[33–35] Therefore, this type of lasing was assigned to be coherent random lasing (RL).[36,37]

As the obtained RL emission behavior was quite chaotic[36] (see Fig. S1 in the ESI†), we averaged RL spectra for each pumping energy over 15 pulses. Then, averaged spectra were plotted, as shown in Fig. 1(c), and from the peak intensity to the excitation pulse energy relations, the threshold conditions were estimated (see the inset in Fig. 1(c) with a characteristic inflection point indicating the lasing threshold). However, even for such an averaging procedure, the estimation of energy thresholds is affected by significant standard deviations.[37] In Fig. 1(d), we depict the threshold conditions as a function of the TCF dye concentration. The lowest threshold was obtained for concentrations ranging between 0.5 and 1 mg mL^{-1}. We also found that when the concentration crossed the value of 1.5 mg mL^{-1}, the precipitation process was observed even by the naked eye. After a while, for all of the samples with the TCF dye concentration $c \geq 1.5$ mg mL^{-1}, the precipitant settled down

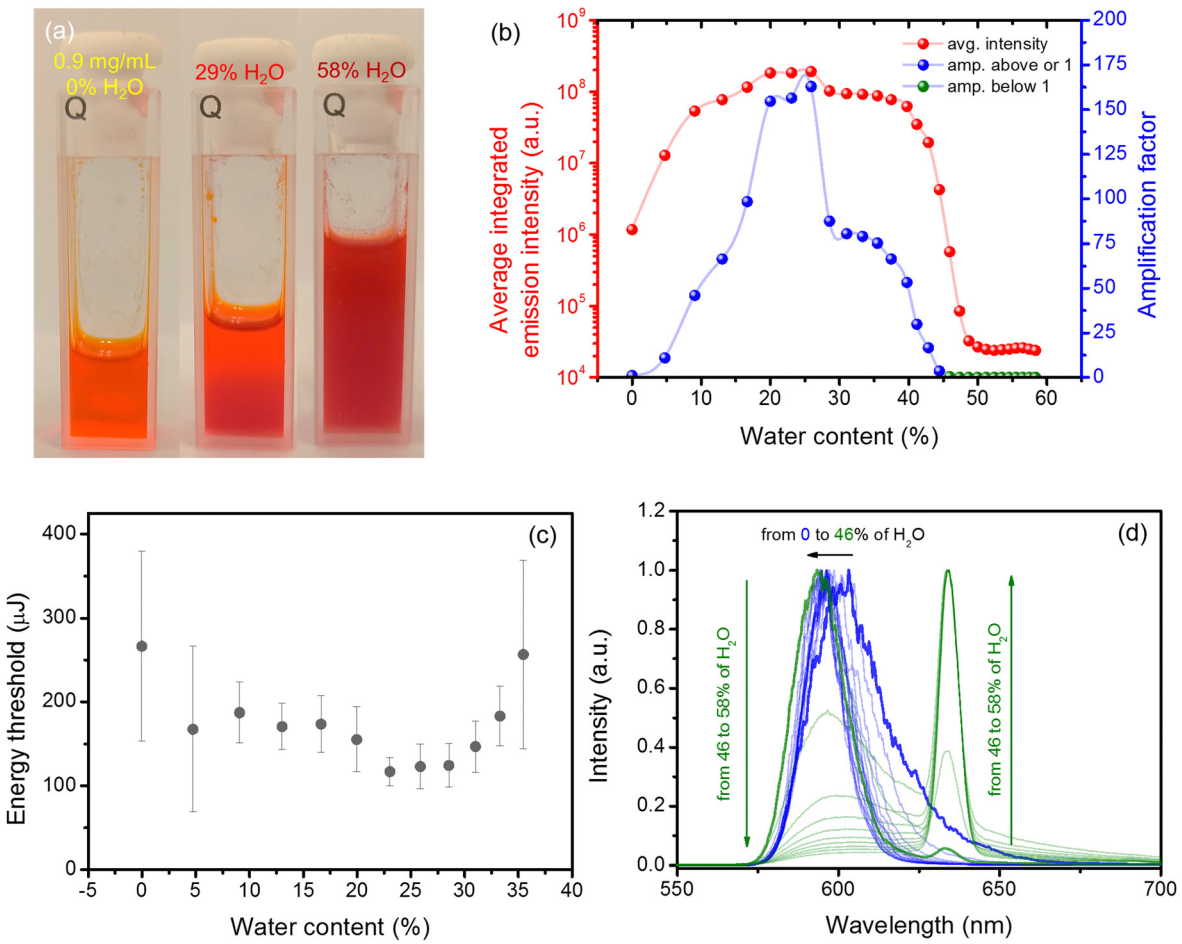

Fig. 2 Photograph demonstrating the difference in color and transparency of 2,4,6-OMe-TCF dissolved in THF at a 0.9 mg mL^{-1} concentration with different amounts of water (a). The average integrated intensity of RL spectra and the amplification factor as the function of the water content (b). Lasing energy threshold dependency on the water content (c). The evolution of the averaged lasing spectrum with increasing water addition (d).

in the form of sediment. Therefore, stirring solutions during laser measurements was mandatory to obtain reproducible results.

However, when the stirring is not enabled, we can clearly see that the precipitate settles down to the vial's bottom for such high concentrations. This process is visualized in the ESI† Fig. S2, where we depicted a photograph showing an 8 mg mL^{-1} solution of TCF just after shaking, with a clearly visible suspension, and the same solution after 15 min. with the clarified supernatant over the sediment. The differences are also visible in the RL spectrum. The clarified supernatant shows an RL spectrum comparable to those reported for our previous measurements, with a maximum emission close to 595 nm. Interestingly, when we excite the suspension after shaking, the RL spectrum is composed of two bands, one at around 595 nm and the second close to 635 nm.

Next, we have focused on the influence of aggregation on the lasing performance caused by the water added to the THF dye solution. We decided to investigate the solution containing 0.9 mg mL^{-1} of the TCF dye because it is very close to the saturation level, and the determined threshold of RL was also relatively low (~270 μJ, which corresponds to ~54 kW). The details of this experiment can be found in the Materials and methods section. An exemplary photograph showing the differences in the solution clarity during the addition of different water amounts is presented in Fig. 2(a). We can see that a transparent orange solution in neat THF turns reddish and hazy when water is added. For such conditions, the RL emission is even more chaotic (see Fig. S3 and Fig. S4 in the ESI†); thus, the averaging was carried out over 600 pulses after each dose of water was added. Fig. 2(b) shows how the integrated intensity (red dots) over averaged RL spectra changes with water addition. The pumping energy for this experiment was kept at the same level and was above the threshold condition of a pristine sample (~285 μJ, which is ~57 kW). We can see a massive change in the RL intensity when water is added to the cuvette.

To better visualize this effect, we have introduced the so-called amplification factor. It is defined as the average integrated intensity for a particular amount of water divided by the average integrated intensity for a pristine solution. Therefore, for no water addition, the value of this factor is equal to 1 by definition. This factor is plotted in Fig. 2(b) with blue dots when it takes values equal to or greater than one and with green dots when its value is below 1. The maximum increase of the RL intensity was reported for the sample that contained 25.9% of water with an average amplification factor of 170. Those results are in accordance with the energy threshold dependence on the water content presented in Fig. 2(c). After crossing this value of water amount, a drop in the integrated intensity was observed. Finally, when the water content reached the value of 44.4%, the integrated intensity was even lower than that reported for the pristine sample, and moreover, another RL band located at a wavelength of 634 nm started to appear. The color of the emission becomes more reddish and dim; however, the light amplification was nonetheless possible. The evolution of averaged RL spectra with the addition of water is shown in Fig. 2(d). The blue spectra represent all measurements for which the intensity was higher or equal to that observed for the pristine sample. The green spectra represent a measurement for which the integrated emission was smaller than reported for the pristine sample. So on average, we obtained two orders of magnitude enhancement of the RL emission for the highest amplification case.

As mentioned before, the previous analysis was carried out for averaged emission spectra. For the dynamic case, when we analyze emission spectra recorded pulse after pulse, the amplification factor can reach a value as high as 544 or as low as 17 for 25.9% of water addition. It must be mentioned that the amplification factor for the dynamic case (Fig. S4, ESI†) was calculated slightly differently. The value of each pulse integrated intensity was divided by the averaged integrated intensity over the whole period when water was not present in the sample (first 600 pulses).

The addition of water is changing not only the RL emission spectrum but also the PL spectrum. The comparison of the PL spectrum of a solution (0.1 mg mL^{-1}), the same solution with 70% of added water, and a powder is shown in Fig. 3(a) with black dashed, dotted, and continuous lines, respectively. The change in the shape of the emission spectrum was observed when water content crossed the value of 60%. This change was also accompanied by a boost in the emission intensity, which is visualized in Fig. S5 in the ESI.† Unlike a solution without any

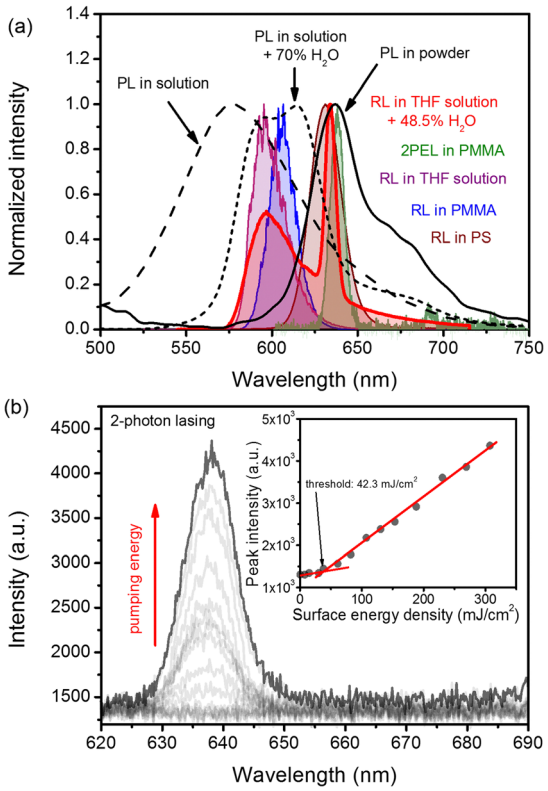

Fig. 3 Comparison of PL and RL spectra obtained for different types of samples (a). Evolution of 2PEL spectra with increasing pumping energy for the PMMA sample with the threshold shown in inset (b).

water addition, the spectrum is composed of two distinct maxima at 592 and 612 nm. The blue-shifted shoulder has a small hump at a wavelength of c.a. ~560–570 nm, which can be assigned to the residual molecular emission of non-aggregated TCF molecules. On the red-shifted shoulder, another small hump located at the wavelength of c.a. ~680 nm is visible. The further increase of the water amount results in complete diminishing of the blue-shifted hump and the increase of the red-shifted one. Interesting results are obtained for a powdered (polycrystalline) sample; the emission is dominated by a considerable maximum located at around 637 nm. The whole spectrum extends between ~600 and 780 nm, with a small hump at the red-shifted shoulder located at ~670–680 nm.

Another type of RL measurement was carried out for samples fabricated in the form of polymeric asymmetric slab waveguides/quasi-waveguides made of polystyrene (PS), and poly(methyl methacrylate) (PMMA) deposited on microscopic support glass slides. The detailed procedure of their fabrication process is available in the ESI† (Sample preparation section). Both samples, made of PS *via* the spin coating technique and made of PMMA *via* drop-casting, are shown in Fig. S6 (ESI†). It is worth noting that both samples show relatively good optical quality; however, the PS sample is more uniform in thickness.

We obtained the following thicknesses: 0.43 ± 0.03 μm and 5.26 ± 0.41 μm for PS and PMMA, respectively.

Both samples were compared in the 1PEL experiment as described in the Materials and Methods in section in the ESI.† From Fig. S7 (ESI†), we can see that the RL threshold obtained for the PS matrix is smaller than that for PMMA and is equal to around 1.9 mJ cm^{-2} (3.8×10^2 kW cm^{-2}). In the case of the PMMA matrix, for which the refractive index is lower than for the glass substrate, the threshold is much higher and is around 15.9 mJ cm^{-2} (3.2×10^3 kW cm^{-2}). Moreover, it is clearly evident that the lasing spectrum for the PS matrix is much more red-shifted and spans between ~ 610 and ~ 650 nm with FWHM ≈ 22 nm. On the other hand, for PMMA, light amplification can be achieved for wavelengths ranging from ~590 to ~620 nm with FWHM ≈15 nm.Here, we determine the threshold conditions using slightly different units, namely mJ cm^{-2} (or kW cm^{-2}). As polymeric films are relatively thin with respect to the Rayleigh length of the beam focus (cylindrical lens with focal length f = 10 cm) we can assume that the excitation volume of polymeric samples has the same cross-section across the layer depth. Therefore the energy fluence or intensity are good parameters to compare with other quasi-2D systems. In previous cases, the 1 cm size of the cuvette, strong absorption, and the scattering causing defocusing make it challenging to determine the real area when the lasing phenomenon occurs. Therefore, we decided to keep the cuvette at the same position during all measurements and to determine thresholds in the manner of total delivered pulse energy or pulse power (for details, see the Materials and Methods section in the ESI†).

Another type of 1PEL measurement was carried out on powdered samples only. The details of the experiment are available in the ESI.† Fig. S8 (ESI†) shows the evolution of the typical RL spectrum upon increasing the pumping fluence. It is worth noting that the gain profile is significantly red-shifted with respect to those exhibited by non-saturated liquid samples and occupies the spectral position at around 637 nm, the same as that reported for powder PL spectrum maximum. The threshold for the powdered sample was equal to 9.4 mJ cm^{-2} (1.9×10^3 kW cm^{-2}).

Finally, we decided to perform the 2PEL experiment using a femtosecond excitation source and the experimental setup described in the Materials and methods section. Additionally, we decided to utilize the thicker sample, made of PMMA instead of a PS-based system, as it exhibited better durability against photodegradation (see the inset in Fig. S7, ESI†). 2PEL was observed above the pumping energy density of 42.3 mJ cm^{-2} (385 GW cm^{-2}) and appeared on the spectrum as the peak located at a wavelength of 638 nm and FWHM ≈ 10 nm (similar to the powdered sample). The evolution of the 2PEL spectrum upon increasing pumping fluence is shown in Fig. 3(b). The inset in Fig. 3(b) shows the peak intensity dependence on the energy density of pumping light with a clearly visible threshold.

In order to gain insight into the precipitation process and types of formed aggregates, we measured the transmission of He–Ne laser light (633 nm) through our liquid samples accompanied by measurements of light scattered at the right angle with respect to the light propagation direction. The selected wavelength of light is not absorbed by our dye, as shown in Fig. 1(a). The details of the experiment are described in the ESI† in the Materials and methods section. In Fig. 4(a), we can see that the transmission for concentration ranging between 0 and 0.35 mg mL^{-1} is nearly constant and equal to ~92% (below 100%, mainly due to the specular reflections from cuvette walls). However, when the concentration crosses the value of 0.35 mg mL^{-1} (the threshold concentration for lasing), the transmission drops down to ~86% (0.63 and 0.9 mg mL^{-1}). Another sudden drop in the transmission is observed when the concentration crosses 0.9 mg mL^{-1}, reaching a value of ~76% for 1.1 and 1.2 mg mL^{-1}. The analysis of scattering, presented in Fig. 4(a), shows that the power of scattered light is growing quasi-linearly up to 0.9 mg mL^{-1}, with a very shallow inflection at 0.35 mg mL^{-1}. This inflection is not visible in Fig. 4(b) due to the scale and is visualized in the ESI† in Fig. S9(a). When the concentration of 0.9 mg mL^{-1} is crossed, we observe a sudden increase in the power of scattered light (from 300 nW to 1.5 μW) due to the presence of macroscopic precipitates. Those results clearly indicate that the oversaturation of solutions starts between 0.9 and 1.1 mg mL^{-1}.

Similar studies were performed for a sample with 0.9 mg mL^{-1} dye as a function of water content. From Fig. 4(b), we see that the consecutive addition of water is not significantly changing the transmission and scattering of up to 33.3% of water content. The changes are very weak; the transmission decreases linearly from ~88% to ~85%, while the power of scattered light increases from ~300 nW to ~400 nW also in a linear manner. The further increase in the water amount results in a drop in transmission and an increase in scattering. The highest decrease in the transmission (and

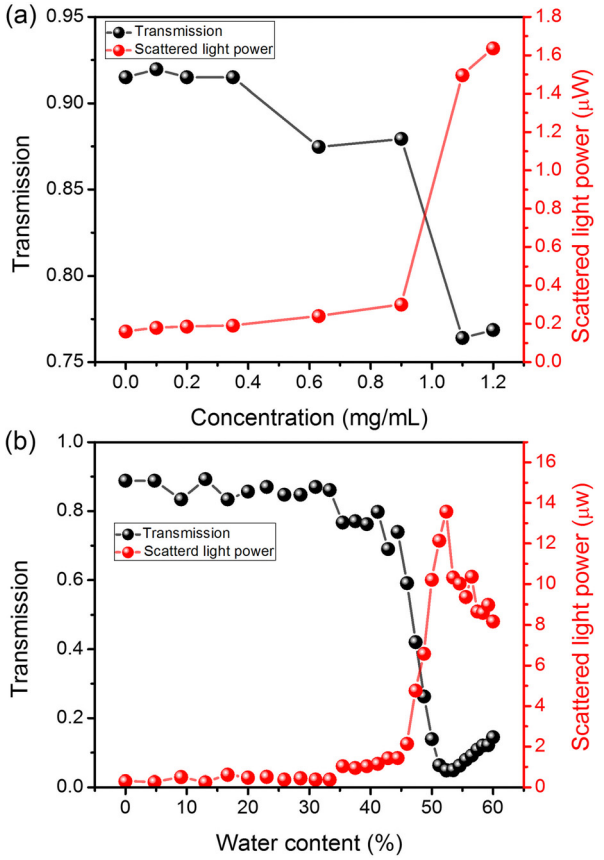

Fig. 4 Light transmission and scatterd light power in function of 2,4,6-OMe-TCF concentration (a) and water content (b).

highest increase of scattering) is reported for water amounts between 44.4% and 53%. When 53% water addition is crossed, we see once again the increase in sample transparency and a decrease in light scattering, which is due to the sedimentation of crystalline particles.

Finally, above mentioned studies were supported by dynamic light scattering (DLS) measurements. The experimental details are available in the ESI† in the Materials and Methods section, and results are also presented in the ESI† in Fig. S9(b). The results carried out for samples with different concentrations of dye have shown too weak scattering signals for analysis, possibly due to the too-small size of aggregates for this technique. Quality reports indicated the presence of sediment for samples with concentrations higher than 0.9 mg mL^{-1}. In the case of measurements concerning water addition, the detection limit crossed 20% of water addition. Small particles of ~1 nm are observed in such cases. The further increase in the water content up to 31% results in a slight growth of particles up to around ~2 nm. When the water addition crosses the value of 39%, FONs are formed, whose sizes vary between 300–900 nm. For 46%, we see the bimodal curve; the size of FONs slightly decreases to around 200–500 nm, but also we can observe the presence of micrometer size particles. For 51% water content, the solution is dominated by particles of micrometer and submicrometer size.

Discussion

The analysis of the lasing threshold dependence on the 2,4,6-OMe-TCF concentration in THF solution indicates that the lasing phenomenon occurs for high concentrations, relatively close to the saturation level (~1.0 mg mL^{-1}, see Fig. 4(a)). Of course, the formation of small aggregates, like dimers, trimers, *etc.*, might start at concentrations far below 1.0 mg mL^{-1}, but sufficient gain related to the formation of the aggregates can be achieved when the concentration reaches or crosses the value of 0.35 mg mL^{-1}. The presence of aggregates was also proven by scattering and transmission experiments, results of which are shown in Fig. 4(a). They clearly indicate that transmission starts to decrease exactly from 0.35 mg mL^{-1}, and the scattering curve has there an inflection point (see Fig S9 (a) in the ESI†).

On the other hand, when the solution becomes oversaturated, the crystals present in the dye powder cannot dissolve. In such cases, the supernatant consists of small aggregates and molecules, while crystals can settle down at the bottom of the cuvette after some time. For example, in the case of a sample containing 8 mg mL^{-1} of the TCF dye, the powder residue forms a clearly visible sediment. When we compare the RL spectra of the supernatant after the sedimentation of the precipitate for this sample (15 minutes after turning off the stirring) with the shaken solution, we will see that the RL spectra are substantially different, as shown in Fig. S2(b) (ESI†). For the spectrum of the supernatant, we can see the RL emission, with the maximum located at ~595 nm, the same as that reported for the solutions with concentrations below the saturation level. However, the second band, located at ~635 nm, appeared when we acquired the RL spectrum from the shaken solution.

Therefore, we link the second band to the crystals' amplified emission, while the RL at 595 nm is due to the small aggregates.

This statement is justified by DLS measurements, which were unable to detect any significant particles in the supernatants, and quality reports indicated the presence of sediment. What is more, the PL and RL spectra shown in Fig. 3(a) are also in accordance with this statement. We can easily see that the PL spectrum of powder is significantly red-shifted with respect to other samples, and its dominant band is exactly matching the position of RL bands reported for powder (Fig. S8, ESI†), sediment (Fig. 2S), and solutions with water fraction higher than, and equal to 46% (Fig. 2(d)).

The results of experiments on RL regarding the influence of water can also be explained in an aforementioned manner. The AIE effect boosts the RL in the band located at 595 nm. The analysis of Fig. 4(b) and Fig. S9(b) (ESI†) shows that in the range of water fractions spanning between 0 and 39%, there are no large aggregates present. In most cases, their sizes are below the detection limit, and finally (for 39%), they grow up to 2 nm. A further increase in water content results in FON formation. Due to the high dispersity and, in general, molecular disorder, we deal with a mix of amorphous and crystalline FONs. According to ref. 22 the emission spectra of both types of FONs have the same shape; thus, they will contribute the same to the resulting PL and RL spectrum. Once the critical water addition

is reached (46% for a solution with 0.9 mg mL^{-1} of the TCF dye), the formation of crystals starts to occur, resulting in an overall drop of the emission intensity and band-switching (to ~635 nm). In order to better visualize this effect, we have depicted the RL spectra acquired for different samples and under different conditions together with PL of a solution, a solution with 70% of water amount, and a dye powder (Fig. 3(a)). The RL spectra almost perfectly match the PL bands that can be assigned to small aggregates for lower amounts of water and the powder PL when RL is obtained from a solution with high water addition. The DLS measurements show the presence of micrometer and sub-micrometer size particles next to FONs. For further increase of water content (51%), microparticles that can be assigned as crystals are dominating the solution.

In general, adding water to the THF-dye mixtures significantly influenced 1PEL intensity and stability. The emission process became chaotic, and the average integrated intensity can be increased even by a factor of 170 (for 25.9% of water addition). Such a massive increase can be caused by the boost of the emission quantum yield[26] and multiple light scattering, which can also provide positive feedback for RL operation. Here, we deal with the RL effect, as the emission spectra are typical for this phenomenon.[36] Hence, the influence of the feedback resulting from the multiple scattering must also be considered in the simulated emission intensity enhancement. Moreover, the disorder at the molecular level leading to a complex interplay between different luminous species is also crucial for the lasing performance. Therefore, the nature of light amplification is not trivial; it involves all of the mentioned mechanisms and cannot be explained only in terms of PL quantum yield enhancement. For example, for a solution with a concentration of 2,4,6-OMe-TCF equal to 0.02 mg mL^{-1}, the 147-fold enhancement of PL was reported.[26] In the ESI,† Fig. S5, we show the PL intensity enhancement by the factor of 55 for the solution with a dye concentration of 0.1 mg mL^{-1}.

Interestingly, a comparison of RL with transmission, scattering, and DLS results indicate that the biggest boost of RL emission is due to the presence of small aggregates of sizes between 1 and 2 nm.

It has to be underlined that the water fraction saturation level (in our case, for a solution containing 0.9 mg mL^{-1} of dye, it is equal to ~46%), the average boost of the RL emission, and the optimal water content, will depend on the initial dye concentration. Therefore, the results obtained for different solution parameters may differ from those which are presented here. Thus, it might be thought that it is still possible to optimize the parameters of the dye solution to obtain much higher amplification factors of the RL emission.

In order to clearly confirm if crystals are responsible for lasing from the band located at around 637 nm, we performed the lasing experiment for the powdered sample (in the form of microcrystals – see Fig. S10 and S11(a) and (b) in the ESI†). This experiment clearly confirmed our suspicion as RL was achieved from the powder at the band located at ~637 nm (see Fig. S8 in the ESI†).

To summarize, small aggregates are responsible for light amplification at the band centered at ~595 nm. Moreover, they are also responsible for the highest amplification, when 26% of water is added to the liquid sample. Further aggregation up to the formation of microcrystals results in band switching to 637 nm.

The 2,4,6-OMe-TCF dye can also be used as a very promising lasing dopant in polymeric environments. In such a case, the influence of the molecular disorder is even more striking as the stimulated emission spectral position is dependent on the matrix and layer deposition method. The analysis of Fig. 3(a) and Fig. S7 (ESI†) indicates that 1PEL for the PMMA sample was achieved at the wavelength of 600 nm, while for the PS-based sample, it occurred at ~635 nm. The strong red shift of emission for the PS sample is mainly due to the better waveguiding effect and reabsorption, but the differences in dye miscibility and matrix-dye interactions cannot be ruled out.

Interestingly, when 2PEL was investigated in the same PMMA sample, the light amplification occurred at the band previously assigned to crystals (~638 nm). It shows that all of the different luminous species are present in polymeric samples (from single molecules to microcrystals) and might be involved in light amplification. This statement can be confirmed by micrographs shown in Fig. S10 in the ESI,† which present a comparison between TCF dye microcrystals in the PMMA layer and the powder sample. However, from emission spectra, we see that for 2-photon excitation, the PMMA-based sample prefers to amplify the light from microcrystals. The obtained threshold of 2PEL is relatively high but comparable to other systems investigated before.[38–41]

Finally, it is worth noting that our polymeric systems were not optimized to exhibit the lowest possible thresholds for 1PEL as well as for 2PEL. Playing with such parameters as different polymeric matrices, thickness, waveguide design, dye concentration, excitation wavelength, scattering strength, *etc.*, or using different resonators, it is possible to decrease the lasing threshold much below the values reported here, as well as to tune the emission wavelength of the resulting laser system.

Conclusions

To conclude, the one- and two-photon excited laser emission was evidenced in samples containing the 2,4,6-OMe-TCF dye, indicating that this compound can serve as a versatile lasing material. It can be used in liquid solutions and as dopants for solid polymeric matrices. The aggregation can be successfully used to boost the efficiency of the light amplification process as the dye shows AIE-like behavior. The AIE phenomenon is crucial and strongly influences threshold conditions, emission intensities, and gain profile spectral positions. Moreover, different luminous species (aggregates and crystals) were evidenced to be responsible for the light enhancement in different spectral regions.

We have shown that the emission intensity can be increased even by a factor of 170. However, we believe that it is still possible to increase this factor even more, as the rate equations

were not yet proposed, and the disorder was also not optimized. The same could be stated about threshold conditions; they can also be optimized by changing the concentration, sample morphology, *etc.* However, the reported ones are still satisfying, *e.g.*, for pumping conditions provided by cheap DPSS lasers of pulsed operation. Moreover, the AIE effect can also coexist with thermally activated delayed fluorescence (TADF),[25] for which ultra-low threshold conditions can be obtained.[42,43] Therefore, the AIE effect can be used next to others to improve the lasing properties of the resulting materials.

The versatility of this compound can also be understood in terms of tailoring of laser properties. For example, elaborating methods that allow controlling the disorder at the molecular level could be very beneficial in developing high-performance and cheap laser materials. Additionally, aggregation-enabled lasing/random lasing may find applications in diagnostics and bio-imaging. Here, the selective ability of different cell organelles stained by AIE dyes could be used for this purpose. Therefore, we believe that novel types of laser-based imaging methods can be developed based on the proposed approach.

Finally, it has to be underlined that 2PEL is not a common phenomenon in organic molecular systems. For typical organic molecular systems, the rate of two-photon absorption becomes significant only for very high concentrations; however, in such cases, the aggregation emission quenching prevents the development of the laser emission. AIE dyes are not affected by this issue. The cross-sections for the two-photon excited fluorescence can thus be increased by aggregation and/or crystallization. Therefore, they are promising candidates for novel multiphoton-excited lasing materials. The presented approach is somewhat different from others, where large molecules are synthesized to fulfill the requirements of a high nonlinear absorption cross-section to ensure laser emission.[44,45]

Here, we have shown that the 2PEL occurs from the dye's crystalline form. This indicates that aggregation/crystallization might be the key strategy to reach the mentioned goal.

Regarding our case, it could be stated that the sufficient gain for 2PEL was due to the dye crystals' involvement.

Author contributions

K. L: investigation, data curation, formal analysis, verification, visualization, writing – original draft, and writing – review & editing; M. D.-M: conceptualization, methodology, validation, and writing – review & editing; Ch. A: conceptualization, resources, and writing – review & editing; Y. B: conceptualization, resources, and writing – review & editing; P. H: methodology, data curation, investigation, formal analysis, validation, visualization, and writing – review & editing; P. F: methodology, investigation, formal analysis, validation, visualization, and writing – review & editing; P. S: investigation, formal analysis, and validation; J. M: conceptualization, methodology, and writing – review & editing; L. S: conceptualization, methodology, formal analysis, data curation, visualization, writing – original draft, supervision, funding acquisition, and project administration.

Conflicts of interest

The authors declare no competing interests.

Acknowledgements

The research was co-financed by the National Science Centre, Poland 2020/39/O/ST5/01865. The authors thank Dr. Maciej Czajkowski for DLS measurements and the PORT Polish Center for Technology Development for XRD analysis.

Notes and references

1 H. Hao, H. Luo, A. Yi, C. Liu, B. Xu, G. Shi and Z. Chi, *Org. Electron.*, 2019, **69**, 281–288.
2 K. Matsuoka, K. Albrecht, K. Yamamoto and K. Fujita, *Sci. Rep.*, 2017, **7**, 41780.
3 Z. Xu, Y. Gong, Y. Dai, Q. Sun, X. Qiao, D. Yang, X. Zhan, Z. Li, B. Z. Tang and D. Ma, *Adv. Opt. Mater.*, 2019, **7**, 1801539.
4 F. De Nisi, R. Francischello, A. Battisti, A. Panniello, E. Fanizza, M. Striccoli, X. Gu, N. L. C. Leung, B. Z. Tang and A. Pucci, *Mater. Chem. Front.*, 2017, **1**, 1406–1412.
5 B. Zhang, J. L. Banal, D. J. Jones, B. Z. Tang, K. P. Ghiggino and W. W. H. Wong, *Mater. Chem. Front.*, 2018, **2**, 615–619.
6 D. Zhao, F. Fan, J. Cheng, Y. Zhang, K. S. Wong, V. G. Chigrinov, H. S. Kwok, L. Guo and B. Z. Tang, *Adv. Opt. Mater.*, 2015, **3**, 199–202.
7 S. Mi, J. Wu, J. Liu, Z. Xu, X. Wu, G. Luo, J. Zheng and C. Xu, *ACS Appl. Mater. Interfaces*, 2015, **7**, 27511–27517.
8 Z.-j Huang, H.-r Mou, J.-p Xie, F. Li, C.-B. Gong, Q. Tang and X.-K. Fu, *Sol. Energy Mater. Sol. Cells*, 2020, **206**, 110293.
9 D. Li, Y. Yang, C. Yang, W. Zhang, Y. Wang, X. Lin, Y. Gao, X. Lv, H. Niu and W. Wang, *Dyes Pigm.*, 2021, **184**, 108799.
10 D. Sengottuvelu, V. Kachwal, P. Raichure, T. Raghav and I. R. Laskar, *ACS Appl. Mater. Interfaces*, 2020, **12**, 31875–31886.
11 J. Qiu, S. Jiang, B. Lin, H. Guo and F. Yang, *Dyes Pigm.*, 2019, **170**, 107590.
12 C. Dai, D. Yang, Y. Hu, Y. Deng, X. Yang and Z. Liu, *New J. Chem.*, 2021, **45**, 4071–4076.
13 X. Yan, M. Remond, Z. Zheng, E. Hoibian, C. Soulage, S. Chambert, C. Andraud, B. Van der Sanden, F. Ganachaud, Y. Bretonnière and J. Bernard, *ACS Appl. Mater. Interfaces*, 2018, **10**, 25154–25165.
14 K. Sun, Y.-L. Zhang, X.-L. Chen, H.-F. Su, Q.-C. Peng, B. Yu, L.-B. Qu and K. Li, *ACS Appl. Bio Mater.*, 2020, **3**, 505–511.
15 X. Wang, L. Wang, X. Mao, Q. Wang, Z. Mu, L. An, W. Zhang, X. Feng, C. Redshaw, C. Cao, A. Qin and B. Z. Tang, *J. Mater. Chem. C*, 2021, **9**, 12828–12838.
16 Y. Tsutsui, W. Zhang, S. Ghosh, T. Sakurai, H. Yoshida, M. Ozaki, T. Akutagawa and S. Seki, *Adv. Opt. Mater.*, 2020, **8**, 1902158.
17 B. Tang, H. Liu, F. Li, Y. Wang and H. Zhang, *Chem. Commun.*, 2016, **52**, 6577–6580.
18 C. Orofino, C. Foucher, F. Farrell, N. J. Findlay, B. Breig, A. L. Kanibolotsky, B. Guilhabert, F. Vilela, N. Laurand,

M. D. Dawson and P. J. Skabara, *J. Polym. Sci., Part A: Polym. Chem.*, 2017, **55**, 734–746.
19 N. Wang, J. S. Evans, J. Mei, J. Zhang, I.-C. Khoo and S. He, *Opt. Express*, 2015, **23**, 33938–33946.
20 M. Durko-Maciag, D. Jacquemin, G. Ulrich, J. Massue and J. Mysliwiec, *Chem. – Eur. J.*, 2022, **28**, e202201327.
21 M. Durko-Maciag, A. Popczyk, M. Rémond, Z. Zheng, Y. Bretonniere, C. Andraud and J. Mysliwiec, *ChemPhotoChem*, 2022, **6**, e202200008.
22 J. Massue, A. Felouat, P. M. Vérité, D. Jacquemin, K. Cyprych, M. Durko, L. Sznitko, J. Mysliwiec and G. Ulrich, *Phys. Chem. Chem. Phys.*, 2018, **20**, 19958–19963.
23 K. H. Cheng, Y. Zhong, B. Y. Xie, Y. Q. Dong, Y. Hong, J. Z. Sun, B. Z. Tang and K. S. Wong, *J. Phys. Chem. C*, 2008, **112**, 17507–17511.
24 X. Li, S. Liu, F. Li and Y. Ma, *Opt. Express*, 2011, **19**, 17691–17696.
25 M. Yu, R. Huang, J. Guo, Z. Zhao and B. Z. Tang, *PhotoniX*, 2020, **1**, 11.
26 M. Ipuy, Y.-Y. Liao, E. Jeanneau, P. L. Baldeck, Y. Bretonnière and C. Andraud, *J. Mater. Chem. C*, 2016, **4**, 766–779.
27 Y. Chen, J. W. Y. Lam, R. T. K. Kwok, B. Liu and B. Z. Tang, *Mater. Horiz.*, 2019, **6**, 428–433.
28 Q. Qi, Y. Liu, X. Fang, Y. Zhang, P. Chen, Y. Wang, B. Yang, B. Xu, W. Tian and S. X.-A. Zhang, *RSC Adv.*, 2013, **3**, 7996–8002.
29 K. Bujak, H. Orlikowska, J. G. Małecki, E. Schab-Balcerzak, S. Bartkiewicz, J. Bogucki, A. Sobolewska and J. Konieczkowska, *Dyes Pigm.*, 2019, **160**, 654–662.
30 L. Čechová, J. Kind, M. Dračínský, J. Filo, Z. Janeba, C. M. Thiele, M. Cigáň and E. Procházková, *J. Org. Chem.*, 2018, **83**, 5986–5998.
31 E. Maçôas, G. Marcelo, S. Pinto, T. Cañeque, A. M. Cuadro, J. J. Vaquero and J. M. G. Martinho, *Chem. Commun.*, 2011, **47**, 7374–7376.
32 M. J. Cho, J. Seo, H. S. Oh, H. Jee, W. J. Kim, K. H. Kim, M. H. Hoang, D. H. Choi and P. N. Prasad, *Sol. Energy Mater. Sol. Cells*, 2012, **98**, 71–77.
33 L. Yin, Y. Liang, B. Yu, Y. Wu, J. Ma, K. Xie, W. Zhang, G. Zou, Z. Hu and Q. Zhang, *RSC Adv.*, 2016, **6**, 85538–85544.
34 Y. Wang, X. Yang, H. Li and C. Sheng, *Opt. Lett.*, 2016, **41**, 269–272.
35 A. Bavali, A. Rahmatpanahi and Z. Niknam, *Opt. Express*, 2022, **30**, 15685–15696.
36 H. Cao, *Waves Random Media*, 2003, **13**, R1–R39.
37 D. S. Wiersma, *Nat. Phys.*, 2008, **4**, 359–367.
38 P. Hanczyc, P. Słota, C. Radzewicz and P. Fita, *J. Photochem. Photobiol., B*, 2022, **228**, 112392.
39 Q. Zheng, H. Zhu, S.-C. Chen, C. Tang, E. Ma and X. Chen, *Nat. Photonics*, 2013, **7**, 234–239.
40 G. S. He, H.-Y. Qin, Q. Zheng, P. N. Prasad, S. Jockusch, N. J. Turro, M. Halim, D. Sames, H. Ågren and S. He, *Phys. Rev. A: At., Mol., Opt. Phys.*, 2008, **77**, 013824.
41 G. Zacharakis, N. A. Papadogiannis and T. G. Papazoglou, *Appl. Phys. Lett.*, 2002, **81**, 2511–2513.
42 Y. Jiang, Y.-Y. Li, X. Liu, H. Lin, K. Gao, W.-Y. Lai and W. Huang, *Chem. Soc. Rev.*, 2020, **49**, 5885–5944.
43 Y. Jiang, P. Lv, J.-Q. Pan, Y. Li, H. Lin, X.-W. Zhang, J. Wang, Y.-Y. Liu, Q. Wei, G.-C. Xing, W.-Y. Lai and W. Huang, *Adv. Funct. Mater.*, 2019, **29**, 180671.
44 Y. Jiang, K. F. Li, K. Gao, H. Lin, H. L. Tam, Y.-Y. Liu, Y. Shu, Ka-L. Wong, W.-Y. Lai, K. W. Cheah and W. Huang, *Angew. Chem., Int. Ed.*, 2021, **60**, 10007–10015.
45 L. Guo, K. F. Li, X. Zhang, K. W. Cheah and M. S. Wong, *Angew. Chem., Int. Ed.*, 2016, **55**, 10639.